

# Deep Neural Networks are Surprisingly Reversible: A Baseline for Zero-Shot Inversion

Xin Dong<sup>1,2\*</sup>, Hongxu Yin<sup>1</sup>, Jose M. Alvarez<sup>1</sup>, Jan Kautz<sup>1</sup>, and Pavlo Molchanov<sup>1</sup>

<sup>1</sup>NVIDIA, <sup>2</sup>Harvard University

xindong@g.harvard.edu, {dannyy, josea, pmolchanov, jkautz}@nvidia.com

## Abstract

Understanding the behavior and vulnerability of pre-trained deep neural networks (DNNs) can help to improve them. Analysis can be performed via reversing the network’s flow to generate inputs from internal representations. Most existing work relies on priors or data-intensive optimization to invert a model, yet struggles to scale to deep architectures and complex datasets. This paper presents a zero-shot direct model inversion framework that recovers the input to the trained model given only the internal representation. The crux of our method is to inverse the DNN in a divide-and-conquer manner while re-syncing the inverted layers via cycle-consistency guidance with the help of synthesized data. As a result, we obtain a single feed-forward model capable of inversion with a single forward pass without seeing any real data of the original task. With the proposed approach, we scale zero-shot direct inversion to deep architectures and complex datasets. We empirically show that modern classification models on ImageNet can, surprisingly, be inverted, allowing an approximate recovery of the original  $224 \times 224$ px images from a representation after more than 20 layers. Moreover, inversion of generators in GANs unveils latent code of a given synthesized face image at  $128 \times 128$ px, which can even, in turn, improve defective synthesized images from GANs.

## 1 Introduction

We focus on the invertibility of an arbitrary pre-trained deep neural network (DNN), *i.e.*, recovering its input from the intermediate representations. The impact of such inversion is two-fold. First, inversion provides insights into how DNNs manipulate and process information at different depths. Inverting an intermediate representation back to the input space unveils how the network filters information and hints at better designing and utilizing deep models for downstream tasks. Second, inversion of widely used DNNs is valuable for analyzing their vulnerability when access to the hidden activations is given.

Mobile and edge devices increasingly rely on DNNs for complex tasks [1–4], while suffering stringent battery and memory constraints [5, 6]. Split computing (SC) has been a popular approach to overcome this via executing the first several layers on devices and the remaining layers on the cloud [7–9]. SC acts as a privacy-preserving way as only features are shared by mobile devices instead of original data [7, 10–14]. Given that no prior work has successfully inverted the released features in the absence of private priors, the paradigm is presumed safe [15–18].

Albeit being important, DNNs’ invertibility remains an ill-posed and challenging problem [19]: it highly depends on model architecture [20], weights distribution [21], and learning objectives [22]. Take the popular activation function in modern DNNs, Rectified Linear Unit (ReLU), for example [23]. It outputs only positive input and zero otherwise. Such a saturation nature prevents anyone from

\*Work done during an internship at NVIDIA.

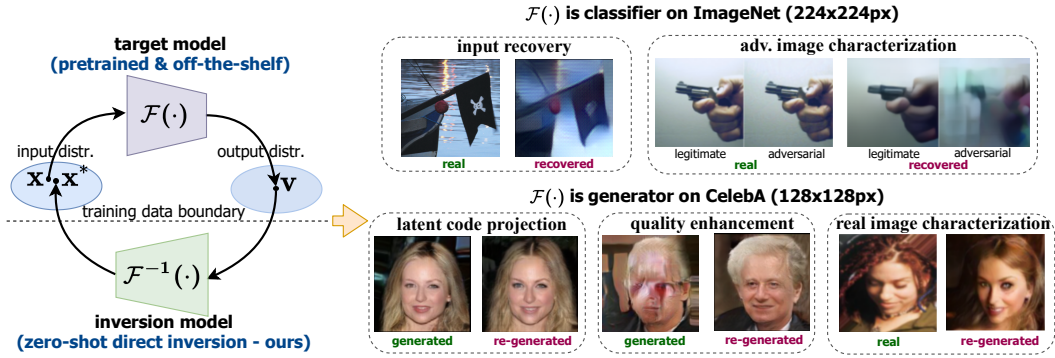


Figure 1: Our method is capable of inverting off-the-shelf pretrained networks in a single step without access to the original data. As a result, an inversion network is learned that enables out-to-input synthesis (Sec. 3). The method is applicable to discriminative (Sec. 4.1) and generative (Sec. 4.2) models trained on complex datasets. Our empirical results shade light on (i) deeper understanding of DNNs in filtering information, (ii) potential defence techniques from adversarial attack, (iii) estimating a latent code for the image generated from GAN, (iv) improving corrupted generated images, and even (iv) potential discriminative feature for real vs generated images (more in Sec. 4). ‘Re-generated’ denotes a new generation from the latent code unveiled by inversion model given the corresponding images on the left.

accurately recovering its input. Linear layers such as convolutional and fully-connected layers are also barely invertible. They can be expressed as a matrix product between weights matrix  $W^T \in \mathbb{R}^{m \times n}$  and layer input. The resulting weights matrix has a left inverse if it has rank  $n$  and a greater-than-one expansion rate  $\frac{m}{n} \geq 1$ . Such condition of expansion rate is hardly satisfied in modern neural networks (e.g., ResNet [24] and RepVGG [25]). What’s more, DNNs are typically trained with discriminative objectives, which are designed to extract class-relevant features and mask out the rest [26–28].

Current approaches of model inversion require specific assumptions to be met to succeed, even for shallow architectures and simple datasets. For example, one direction of works provides theoretical proof of the invertibility assuming the weights of DNNs are random-like [19, 29, 30], and expansion rates are larger than a certain constant [21, 31]. However, these conditions are hardly satisfied for existing trained DNNs [32, 33]. Other works formulate the inversion problem as a generative task [34–37]. They either leverage a pre-trained generative adversarial network (e.g., BigGAN [38]) or train a GAN from scratch with large amounts of real data. The generator in the GAN acts as the inversion model to recover input given the hidden activations. In this scenario, knowledge and access to the pre-trained GAN or original dataset are necessary. This makes inversion obsolete in various application scenarios, e.g., in practice, no pre-trained GAN nor the massive amount of original images are provided amid cost, privacy, and proprietary concerns.

This paper considers the problem of *zero-shot model inversion*: we study the viability to learn an inversion model that faithfully reverses the original function mapping, given only a target pre-trained model without access to original training data. Our proposed method *unifies* the inversion for both discriminative and generative models as shown in Fig. 1. To overcome the increased complexity and non-linearity of the target model as depth increases, we propose a divide-and-conquer inversion method that partitions the inversion into sequential layer/block-wise inversion sub-problems. To support optimization of modules in the inversion model, we exploit synthetic data generated via minimizing the discrepancy between noise input’s feature statistics and ones stored in batch normalization (BN) [39–41]. With synthetic data proxies, we are able to optimize the inversion model to enforce feature embedding similarity with respect to the original counterpart. We call it cycle consistency-guided inversion. Combining aforementioned techniques enables us to successfully scale zero-shot model inversion to deep architectures and complicated datasets without assumptions on model or dataset priors.

In summary, we make the following contributions: (i) We propose a new inversion paradigm based on a divide-and-conquer strategy and a cycle-consistency loss. (ii) We demonstrate that the method generalizes to both discriminative and generating models, even for complex datasets (i.e., ImageNet [42] and CelebA [43]), surpassing state-of-the-art baselines. (iii) We analyze inversion insights, including image recovery, quality enhancement, latent code projection, and adversarial sample characterization.

## 2 Related Work

We next investigate previous work and cast them into four categories: invertible neural networks, analytical inversion, generative inversion, and input optimization based inversion.

**Invertible Neural Networks.** Invertible neural networks (INN) [20, 44–47] are a family of neural networks which can be treated as one-to-one function approximators because of their special architecture and restricted weights distribution. For example, i-RevNet [20] consists of well-designed RevBlocks, which are interleaved with convolution, reshuffling, and partitioning, and i-ResNet [44] adds Lipschitz condition of weights to ResNet [24]. Earlier literature on flow-based generative models [48–50] shares similar design principles.

**Analytical Inversion.** Most of INNs have to rely on exotic architectures and regularization, thus cannot be applied on standard model architectures. Analytical inversion relaxes the constraint on model architecture and studies the theoretical invertibility of standard feedforward neural networks [51]. For example, [19, 29] theoretically show that the approximate reverse of a feedforward layer can be obtained by taking the transpose of weights matrix, based on the hypothesis that weights in the target network are random-like, which is not always held for a pre-trained network [32, 33]. Despite the simplicity, these methods can only scale to CIFAR-10 level, and the recovered images are noisy. [29], in addition, makes a strong assumption that the activation function is concatenated ReLU [52] which keeps the positive and negative values separately. Besides discriminative models, [21, 53] investigate the theoretical invertibility of the deep generative model. [21] indicates that the per layer inversion can be achieved through linear programming in polynomial time if weights are random-like and the layer output dimension is larger than double that of input, and empirically inverts a simple generator on the MNIST dataset.

**Generative Inversion.** Despite of the great progress of analytical inversion, there is still a discrepancy between conditions of theories and modern pre-trained models. As a learning-based and data-driven approach, generative inversion aims to learn a generative model that reverses the target model’s input-output mapping. [35, 54] leverage a pre-trained generator (*e.g.*, BigGAN [38]) as the ‘learned prior’, to optimize the latent space of a generator to maximize the activation of target network. If exquisite pre-trained generators are not accessible, a generative adversarial network can be trained on the original dataset of the target model [36]. The generator takes features as input and outputs the reconstructed images, and the binary discriminator distinguishes real and reconstructed images to compete with the generator. The dependence on the pre-trained generator, the original dataset, and unstable adversarial learning limits the practicability of generative inversion. In addition, at most 6 layers in relative shallow architecture (*i.e.*, AlexNet) are inverted in the mentioned works, yet scalable to modern deep architectures.

**Input Optimization Based Inversion.** Given an arbitrary pre-trained discriminative model such as classifier, [40, 55–58] show that one can reveal certain information of training set by optimization to match pre-stored statistics or maximum activation of neurons. However, these methods are all designed for untargeted model inversion and cannot reconstruct the input faithfully given the feature embedding. In addition, these methods remain computationally heavy.

**Autoencoder.** Model inversion is also related to autoencoders [59, 60] given a similar functionality of target and inversion models, to an encoder-decoder pair. However, the encoder and decoder in an autoencoder are trained jointly with a massive amount of data in an end-to-end manner. In our case, only an individually pre-trained target model is accessible. Aligning with the previous finding of layer-wise training of autoencoder (*e.g.*, deep belief network [61, 62]), and we also find greedy layer-wise training beneficial for inversion model training as detailed in Sec. 3.3.

To summarize the above literature, one common trend is that researchers continually reduce the assumptions made by previous studies, for example, exotic architectures, random weights distribution, and specific layer expansion rate. In this paper, we focus on direct model inversion with *minimal* assumptions, *i.e.*, without original dataset nor exquisite priors but only the target pre-trained model. We unify the inversion of both discriminative and generative deep models and scale the inversion to deep architectures and complex datasets.

Table 1: Comparison of our approach with prior work.

	DeePSIM [34, 36]	IHT [29]	i-ResNet [44]	PlugPlay [35]	DeepInversion [40]	Ours
Zero-shot		✓	✓		✓	✓
No pre-trained prior	✓	✓	✓		✓	✓
No adversarial training		✓	✓	✓	✓	✓
Single-pass inversion	✓	✓	✓		✓	✓
No exotic arch./weight constraint	✓			✓	✓	✓
Unify inversion of multiple models						✓

### 3 Method

We first formulate the problem and then describe the proposed inversion method. Consider a multi-layer neural network (discriminative or generative) as a transfer function composed of  $L$  layers,  $\mathcal{F}_{1:L}(\mathbf{x}) := \mathcal{F}_L \circ \mathcal{F}_{L-1} \circ \dots \circ \mathcal{F}_1(\mathbf{x})$ , trained on the dataset  $\mathcal{D}$ .  $\mathcal{F}_k$  is the  $k^{\text{th}}$  parameterized layer that may include its associated batch normalization and activation. Unless otherwise specified, we consider the widely used  $\text{ReLU}(\cdot) = \max(0, \cdot)$  as the activation function. However, all the results in this paper can be extended to  $\text{LeakyReLU}(\cdot) = \max(0, \cdot) + c \min(0, \cdot)$  or other variants.  $\mathcal{F}_{k:l}$  is the sub-network from  $k$ -th to  $l$ -th layers, *e.g.*,  $\mathcal{F}_{1:1}$  is the first layer and  $\mathcal{F}_{1:L}$  is the whole network.

In this paper, we consider the following problem: given a pre-trained network  $\mathcal{F}_{1:L}$ , is it possible to learn its (approximate) reverse function  $\mathcal{F}_{1:L}^{-1}$  without access to  $\mathcal{D}$ ? This is practical for scenarios where original data is not available and learning a direct decoder is not possible. More specifically, we expect to learn a new function  $\mathcal{F}_{1:L}^{-1} : \mathcal{F}_{1:L}(\mathbf{x}) \rightarrow \mathbf{x}' \approx \mathbf{x}$ , where  $\mathbf{x}'$  is the recovered input.

#### 3.1 Divide-and-Conquer Inversion

DNNs have a compositional structure, consisting of layers or even blocks operating on the propagated tensor called a feature map. Several studies have revealed that neural networks produce more complicated feature maps of higher non-linearity and capacity as the depth increases [63–66]. As a result, the difficulty of DNN inversion was reported in previous work [29, 36, 34, 53].

To circumvent the difficulty of approximating all stacked layers jointly from scratch, we first partition the overall inversion problem into several layer-(or block-)wise inversion sub-problems before integrating them together for refinement. To this end, we introduce a simple yet effective inversion strategy called **Divide-and-Conquer Inversion (DCI)** that progressively inverts the computational flow of DNNs and gradually refines them. Different from a direct end-to-end inversion, DCI has two advantages: (i) a single layer (or block) has less non-linearity and complexity, thus is easier to be inverted; (ii) DCI provides richer supervision signal across layers (or blocks), while the overall inversion only utilizes supervision at the two ends of the target model. Both strengths make the optimization more effective, stable, and data efficient.

Starting from the first layer, DCI inverts each layer  $\mathcal{F}_k$  with two simultaneous goals: (i) inverting the target layer  $\mathcal{F}_k$ , and (ii) ensuring that newly inverted layer  $\mathcal{F}_k^{-1}$  works well jointly with all previously inverted layers  $\mathcal{F}_{1:(k-1)}^{-1}$ . The necessity of the second objective comes from the non-exact inversion and small deltas that are amplified when propagated. Therefore we adjust representations according to the accumulated error. For the first objective, we minimize the layer reconstruction loss,

$$\mathcal{L}_{\text{layer}} = \|\mathbf{u}_k - \mathcal{F}_k^{-1}(\mathcal{F}_k(\mathbf{u}_k))\|_1, \quad \mathbf{u}_k = \mathcal{F}_{1:(k-1)}(\mathbf{x}), \quad (1)$$

where  $\mathbf{u}_k$  is the input of the target layer. As for the second objective, we aim to ensure the reconstruction quality of the current temporary “overall” inversion model up to the layer  $k$  such that  $\mathcal{F}_{1:k}^{-1} = \mathcal{F}_k^{-1} \circ \mathcal{F}_{1:(k-1)}^{-1}$ . This translates into minimizing the distance between inverted input  $\mathbf{x}' = \mathcal{F}_{1:k}^{-1}(\mathcal{F}_{1:k}(\mathbf{x}))$  to the original input  $\mathbf{x}$ , where we introduce another loss term for this purpose:

$$\mathcal{L}_{\text{img}}(\mathbf{x}, \mathbf{x}') = \|\mathbf{x} - \mathbf{x}'\|_1, \quad \mathbf{x}' = \mathcal{F}_{1:k}^{-1}(\mathcal{F}_{1:k}(\mathbf{x})). \quad (2)$$

#### 3.2 Cycle-Consistency Guided Inversion

We further re-exploit the target model for stronger inversion guidance amid the unique setup of the inversion problem. As we reverse the computation of the target model, this forms a natural loop with the original computation flow. Inspired by perceptual metric [67] and cycle-consistent image translation [68], we explore cycle consistency to measure the quality of reconstructed inputs by re-checking them with the target model. Intuitively, if the reconstructed input is faithfully and semantically close to the original input then the direct model should produce similar, if not exact, feature responses at all layers. To this end, we cycle the reconstructed input back to the direct (target) model, and minimize the distance between features of the reconstructed input and original input at various depth. The cycle consistency for inversion is formally defined as follow:

$$\mathcal{L}_{\text{cyc}}(\mathbf{x}, \mathbf{x}') = \sum_{l=1}^L \|\mathcal{F}_{1:l}(\mathbf{x}) - \mathcal{F}_{1:l}(\mathbf{x}')\|_1. \quad (3)$$



This enables a full utilization of the features from the original input twice to provide richer supervision during optimization of inversion model. In the layer reconstruction loss (Eq. (1)), we use features of the original input  $\mathcal{F}_{1:(k-1)}(\mathbf{x})$  as the reconstruction objective. In addition, the cycle consistency loss (Eq. (3)) also uses features of the original input as a reference and enforces the inverted input to have similar features as the original input. With the above losses, the final optimization objective for an inversion layer can thus be expressed as

$$\mathcal{L}_k = \mathcal{L}_{\text{layer}} + \mathcal{L}_{\text{img}} + \alpha \mathcal{L}_{\text{cyc}}, \quad (4)$$

where  $\alpha$  is a hyper-parameter.

### 3.3 Training Strategy

DCI divides the computation of a feed-forward neural network into several parts and inverts the computational flow progressively. One straightforward strategy is to sequentially optimize each individual inversion module  $\mathcal{F}_k^{-1}$  starting from the first (*i.e.*, input) layer  $\mathcal{F}_1^{-1}$ . We observe that the inversion error will accumulate as we move deeper in the model. To mitigate this accumulation issue, we utilize an improved training strategy. After the optimization of a certain inversion module  $\mathcal{F}_k^{-1}$ , we further take all previous inversion modules into consideration and fine-tune all layers up to  $k$ , *i.e.*,  $\mathcal{F}_1^{-1} \circ \dots \circ \mathcal{F}_{k-1}^{-1} \circ \mathcal{F}_k^{-1}$ , with the same loss  $\mathcal{L}_k$  to reduce the accumulated inversion error. When  $k = 1$ , we skip this fine-tuning because there is no inversion model before  $\mathcal{F}_1^{-1}$ .

### 3.4 Data Sampling

One remaining challenge to optimize inversion modules with Eq. (4) is input data  $\mathbf{x}$ . When the target model is a generative model (*i.e.*, the generator of a generative adversarial network), it is effortless to get input data by sampling random latent codes from a Normal (or Uniform) distribution. However, when the target model is an image classification model, it is not feasible to know or sample images from the underlying image distribution. Although one can model a superset of input images by sampling each pixel independently from a uniform distribution  $U(0, \mathcal{I})$ , this superset would be too different from the real data distribution, and in practice too loose as input proxies [40].

It may seem that the original training data is needed for fine-tuning of the inverted model, but the model itself is more than sufficient to provide enough guidance. Inspired by the progress in adversarial-free generative models [69, 70] and data-free knowledge distillation [40, 41], we re-use these techniques to generate a small subset for finetuning. The method we choose minimizes the discrepancy between features statistics of synthetic data  $\hat{\mathbf{x}}$  and statistics stored in batch normalization (BN) layers:

$$\min_{\hat{\mathbf{x}}} \text{CE}(\hat{\mathbf{x}}, \hat{\mathbf{y}}) + \underbrace{\sum_l \|\mu_l(\hat{\mathbf{x}}) - \text{BN}_l(\mu)\|_2 + \sum_l \|\sigma_l^2(\hat{\mathbf{x}}) - \text{BN}_l(\sigma^2)\|_2}_{\text{the key loss term: feature statistics matching loss}} + \lambda \mathcal{R}_{\text{img}}(\hat{\mathbf{x}}), \quad (5)$$

where  $\mu_l(\hat{\mathbf{x}})$  and  $\sigma_l^2(\hat{\mathbf{x}})$  are features statistics computed at the  $l$ -th layer.  $\text{BN}_l(\mu)$  and  $\text{BN}_l(\sigma^2)$  are their corresponding moving averages stored in BN layers.  $\text{CE}(\cdot, \cdot)$  is the cross entropy between  $\hat{\mathbf{x}}$  and a randomly assigned label  $\hat{\mathbf{y}}$ , and  $\mathcal{R}_{\text{img}}$  is a secondary image regularization like total variance to make derived images more natural [40]. Minimizing the discrepancy of features' statistics between synthetic data and real data (*i.e.*, BN statistics) is equivalent to reducing the integral probability metric [69–71] between distributions of synthetic data and real data<sup>2</sup>. Thus, the synthetic data can be treated as data from a distribution which is close to the underlying real data distribution and thus can act as a reasonable proxy for the model inversion task.

Naively combining BN-guided data synthesis and other existing inversion approaches is suboptimal due to the following reasons:

- Prior work [36, 54] train a generator (in a GAN framework) as the inversion model, whereas the GAN training is very sensitive and challenging given only synthetic data [72–74]. The resulting efficacy falls short to DCI, as we will show later in Sec. 4.3.
- Prior work [35, 36, 54] usually require the whole training set (more than 1M images) to train the GAN for inversion. Yet deriving massive synthetic data remains slow [40].

<sup>2</sup>We detail this intuitive justification in appendix.

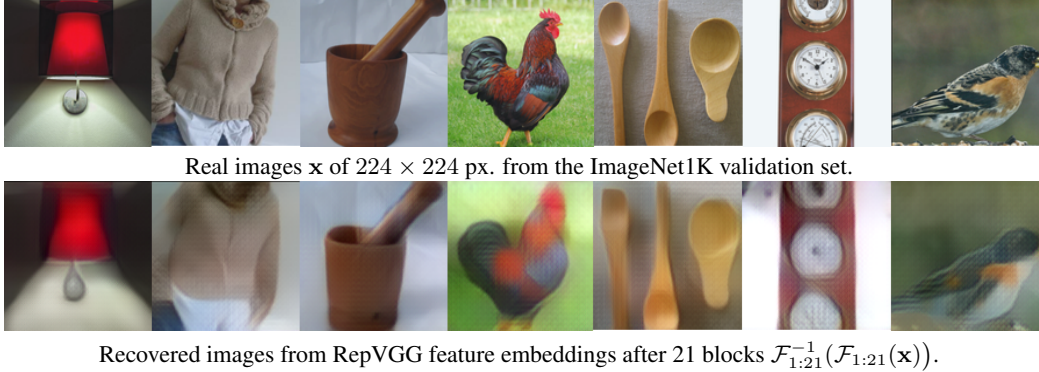


Figure 2: ImageNet inversion results given only a pretrained RepVGG without additional information. Note that recovered images have contextually correct backgrounds, in realistic scenarios, of close proxy to real samples. Best viewed in color.

In contrast, without any adversarial learning, DCI does not have the above disadvantages when using synthetic data because of its progressive inversion nature and cycle consistency supervision. DCI is data-efficient and can be enabled by only 5K synthetic images.

## 4 Experiments

We next demonstrate the efficacy of our method on inverting discriminate and generative models.

### 4.1 Classifier Inversion on the ImageNet1K Dataset

We first study inversion of the classifiers. For this set of experiments, we consider the inversion of RepVGG [25] that is one of the state-of-the-art classification models with a deep yet mathematically neat architecture. It has a ResNet-like [24] multi-branch topology during training, and a mathematically equivalent VGG-like [75] inference-time architecture, achieved by layer folding. Specifically, we target a RepVGG-A0 [25] that has 22 convolution layers, each of which consists of a  $3 \times 3$  convolution, a ReLU, and a folded BN layer, yielding a 72.41% top-1 validation accuracy on ImageNet<sup>3</sup>. We invert one convolution layer at a time using our DCI strategy, starting from the input layer. Each inversion layer mimics its corresponding target counterpart. Each inversion layer is optimized via Adam [76] for 6K iterations. We use 5K synthetic images as detailed in Sec. 3.4 for the optimization. See appendix for additional experimental details.

**Main Inversion Results.** Fig. 2 shows inversion results on ImageNet1K. Remarkably, inversion recovers very close pixel-wise proxy to the original image from deep embedding outputted by the 21-th layer<sup>4</sup>, preserving original semantic and visual attributes, including color, orientation, outline, and position.

#### Inversion at Different Layer Depths.

As noticed, edges are blurred in inverted images, likely caused by information filtering due to the classification nature of the model. To dig deeper into this hypothesis, we visualize the inverted images from different depths of the target model in Fig. 3. As the depth increases, inverted images become more

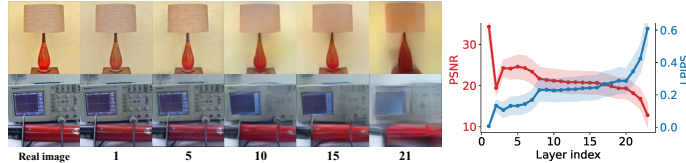


Figure 3: Inversion from features at increased depths. (Left) ‘0’ donates real image. Number indicates layer depth. (Right) PSNR and LPIPS at various layer depths. Shaded region is the standard deviation across ImageNet testing set.

<sup>3</sup>Based on the author CVPR’21 released repo and models at <https://github.com/DingXiaoH/RepVGG>

<sup>4</sup>The spatial size of this embedding is (14, 14).

blurry, losing more details. To quantify the changes, we also provide peak signal-to-noise ratio (PSNR) [77] and learned perceptual metric (LPIPS) [67] in Fig. 3 (right) that is consistent with the qualitative observation.

One intriguing fact shown in Fig. 3 resides in a consistent preservation of high level information across most layers, challenging prior security arguments in split computing [7, 10–14]. For example, as shown in Fig. 3, we can achieve nearly perfect recovery from outputs of the 5-th layer (with spatial size  $28 \times 28$ px) that already past three stride-2 convolutions perceived as lossy operations. We also find that increasing the depth is not always effective in making inversion harder, hence hinges on easy mitigation of such risks via deploying deeper sub-nets on devices. As shown in Fig. 3 (right), using features from the 8-th to 16-th layers still results in recovered images of similar quality in terms of PSNR and LPIPS. Finally, we find that the last two layers dramatically degrade the inversion quality. One can still recognize the class of inverted images after the penultimate (*i.e.*, the 22-th convolution) layer. However, if we invert features after the final (*i.e.*, the fully-connected) layer, only the predominant color is recognizable<sup>5</sup>. This may indicate that class-invariant information is quickly filtered out towards the end of the model while the initial stages focus on feature extractions. This is also in line with observations in transfer learning [78–82] and self-supervised learning [83–85].

### Recovering Adversarial Samples.

We next leverage inversion to understand mechanism of adversarial images [87]. During the crafting process of adversarial samples, adversarial perturbation is optimized to maximize the tangle of network prediction [88]. We find that inversion model has discrepant behavior for randomly (Gaussian noise) perturbed images and adversarially perturbed ones. As shown in Fig. 4, randomly perturbed images share close proxy semantics with original images. However, when we do inversion from features of adversarial samples crafted by PGD [86], the recovered images reveal high-order chaos. This occurrence implies that not only the prediction results but also the intermediate features are disrupted by adversarial samples. The visualization of feature maps corresponding to images with random and adversarial perturbations in the appendix reinforces the above finding. This provides heuristic insights on large-scale dataset to prior work that argue random perturbation with same magnitude won’t disturb the network [89, 90]. The discrepant inversion behaviors for adversarial and legitimate samples may inspire defense methods.

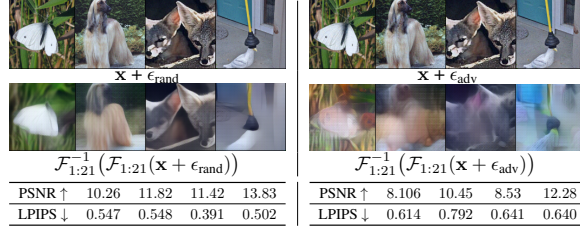


Figure 4: For each image group: top left is legitimate image (base  $\mathbf{x}$  + random perturbation  $\epsilon_{\text{rand}}$ ), top right is adversarial image (base  $\mathbf{x}$  + adversarial perturbation  $\epsilon_{\text{adv}}$  [86]). Both perturbations are of the same magnitude. Image pairs are vertically aligned. Tables match image pairs left to right.

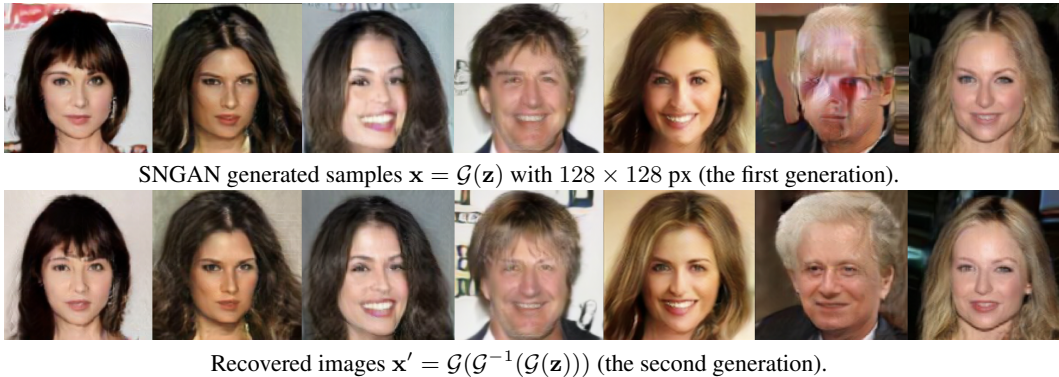


Figure 5: CelebA inversion results. The recovered latent codes unveil images that are very close to the original samples, with similar visual feature, style, and orientation. Inversion improves the quality of some defective samples.

<sup>5</sup>We include inversion results from features of the 22-th convolution layer and final fully-connected layer in the appendix.

## 4.2 GAN Inversion on the CelebA Dataset

We next shift to inversion of generative models. For this experiment we focus on the popular SNGAN architecture that has 2.72 Inception Score (IS) on the CelebA dataset of  $128 \times 128$ px resolution [91]. The SNGAN has 17 layers, including one fully-connected layer at the beginning, one convolution layer at the end, and 5 residual blocks. Each residual block consists of 3 convolution layers.<sup>6</sup> We break the inversion of the whole SNGAN model into inversion of the fully-connected layer, the last convolution layer, and 5 residual blocks with the optimization objective in Eq. (4) and the training strategy in Sec. 3.3. For mathematical consistency with prior GAN literature, we use  $\mathcal{G} : \mathbf{z} \rightarrow \mathbf{x}$  to indicate the target generator instead of  $\mathcal{F}$ .  $\mathbf{z}$  denotes sampled latent code that generates  $\mathbf{x} = \mathcal{G}(\mathbf{z})$ . We aim to learn  $\mathcal{G}^{-1}$  that faithfully reconstructs  $\mathbf{z}$  given  $\mathbf{x}$ , a problem that has large practical impacts (e.g., image compression) but remains challenging [21, 92].

**Main Inversion Results for Latent Code Recovery.** Fig. 5 visualizes our inversion results of the target generator. To demonstrate efficacy we first use the inversion model to recover latent codes, and then pass the recovery back to the generator. Without bells and whistles, the second generation images faithfully align with the first generation. In addition, recovered faces are visually very similar to the original targets. One interesting observation is that the inversion and re-generation process  $\mathbf{x}' = \mathcal{G}(\mathcal{G}^{-1}(\mathcal{G}(\mathbf{z})))$  purify the secondary attributes such as backgrounds, but preserve main attributes of the faces. This further indicates that our inversion takes semantic information into consideration on account of the cycle consistency guidance.

**Interpolation of Recovered Latent Codes.** To show validity of recovered latent code space, we conduct linear interpolation between recovered latent codes as in Fig. 6. This signifies that the recovered latent codes fit well in the input space of SNGAN, sitting on smooth transitions between adjacent samples.

**Improving Defective Generated Images.** One favorable concomitant of inversion and re-generation is that the defective first-generation images can be greatly after re-projection, shown in Fig. 7. Here a first generation image is generated by SNGAN starting from a randomly sampled latent code. The random latent code, as well as the first generation image, could be outliers, slightly diverging from the distribution of normal input. Since the inversion model is trained for the output-to-input mapping, it finds the closest in-distribution latent code for the original outlier latent code during recovery, hence improves image quality.

**Real vs. Generated Images.** All the above experiments are conducted on the first generation images from SNGAN. We next check upon whether the inversion model has distinct behaviors for real images, as noticed by Kerras *et al.* latent code per real image results in a distant synthesis than the original sample [92]. For a fair comparison, we first save both real images and generated images in the format of PNG [93] and use strictly the same inversion pipeline for both of them.

Although SNGAN is trained to map a base distribution (e.g., Normal distribution) to the underlying distribution of real images, there is still a discrepancy between SNGAN’s output distribution and the

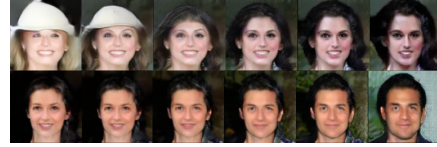
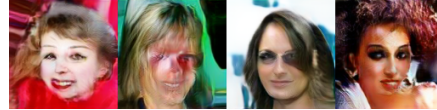


Figure 6: Linear interpolation of inverted latent codes  $\mathcal{G}(\mathcal{G}^{-1}(\mathbf{x}_1) \rightarrow \mathcal{G}^{-1}(\mathbf{x}_2))$ .

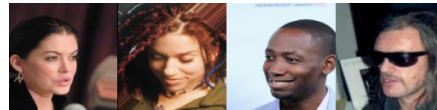


(a) Defective SNGAN-generated images  $\mathcal{G}(\mathbf{z})$ .



(b) Improved images via inversion-reprojection  $\mathcal{G}(\mathcal{G}^{-1}(\mathcal{G}(\mathbf{z})))$ .

Figure 7: Inversion improves the failure cases of SNGAN-generated samples.



(a) Real images  $\mathbf{x}$  from the CelebA validation set.



(b) Re-synthesized latent codes from inversion  $\mathcal{G}(\mathcal{G}^{-1}(\mathbf{x}))$ .

Figure 8: Inverting real images. Unlike generated images, real images are changed after inversion.

<sup>6</sup>Based on implementation and models at <https://github.com/kwotsin/mimicry/>





Figure 9: Qualitative comparison to prior inversion methods.

underlying distribution. We observe that the inversion model is able to capture such distribution discrepancy, demonstrating varying behaviors on the generated and real images, as shown in Fig. 8. The inversion model can still faithfully invert generated images, but shift real images and alter the style after inversion and re-generation. Instead real images and their second generation merely share orientation and color. This may inspire future work on detecting deep fake images [94, 95].

### 4.3 Comparison to Prior Work

Next, we compare our method with other approaches under the zero-shot model inversion setup, that either optimize an auxiliary network ((a) DeePSiM [36]) or input tensors ((b) DeepDream [55] and (c) DeepInversion [40]). We include their detailed setups in Appendix.

We show both qualitative comparison in Fig. 9 and quantitative results in Table 2.

The inferior result of DeePSiM (trained with synthetic data) demonstrates the incompatible combination of previous generative inversion approaches [35, 36, 54] and BN guided data synthesis as discussed in Sec. 3.4. DeepDream yields unrecognizable images compared to our method, while DeepInversion results in improved features and semantics even though a gap remains between recovered and original images. Both DeepDream and DeepInversion require 20K forward and backward passes to optimize inputs – while our method only needs one forward pass through the inversion model, hence is much more efficient.

Table 2: Quantitative comparison to prior methods.

Method	Inference Time <sup>†</sup> (s) ↓	PSNR ↑	LPIPS ↓
DeepDream [55]	0.55K	9.53	0.90
DeepInversion [40]	1.92K	10.93	0.60
<b>This work</b>	<b>0.015</b>	<b>18.83</b>	<b>0.44</b>

<sup>†</sup> Inference time measured on NVIDIA V100 GPU at batch size 4.

### 4.4 Inverting More Architectures on ImageNet1K

To demonstrate the general applicability of the proposed method, we next show inversion results for additional networks on the ImageNet dataset, covering varying architectures (ResNet-18 and ResNet-50) and training recipes (standard [24] and self-supervised [96]).

**Inverting ResNet-18.** We start with ResNet-18 inversion. For this experiment we base the network on the implementation and pre-trained model of ResNet-18 from the PyTorch model zoo [97]. ResNet-18 contains 8 units of BasicBlock, each of which consists of two convolution layers (with BN and ReLU) and a shortcut connection. BasicBlock has a multi-branch architecture because of the existence of shortcut connection. We invert the BasicBlock as a whole unit. The first four sequential layers in ResNet-18 are convolution, BN, ReLU, and max pooling layers. Since it is impossible to invert a max pooling without additional information [98], we invert the sequence of the first four layers as a whole block, which we refer to as the initial block. Same as before, each inversion block mimics its corresponding target counterpart but with reversed input and output dimensions.

Fig. 10 shows inversion results of pre-trained ResNet-18 on ImageNet. With the proposed method, we are able to recover recognizable input images after up to 7 blocks (the initial block and 6 BasicBlock’s) that contain 15 convolution layers and one max pooling layer in total. We observe inversion can still faithfully restore semantically correct images of high fidelity that contain similar visual details to original counterparts.

**Inverting ResNet-50 (standard [24] and self-supervised MoCo V2 [96]).** We next move to invert a deeper architecture as ResNet-50. For additional insights to network behavior, we study inversion of both a normally trained network as in [24], and the recent self-supervised trained network as in MoCo



Real images  $\mathbf{x}$  of  $224 \times 224$  px. from the ImageNet1K validation set.



Recovered images from ResNet-18 feature embeddings after 15 convolution layers  $\mathcal{F}_{1:15}^{-1}(\mathcal{F}_{1:15}(\mathbf{x}))$ .

Figure 10: ImageNet inversion results given only a pretrained ResNet-18 without original data. Note that recovered images have contextually correct backgrounds, in realistic scenarios, of close proxy to real samples. Best viewed in color.



Real images  $\mathbf{x}$  of  $224 \times 224$  px. from the ImageNet1K validation set.



Recovered images from ResNet-50 (standard) feature embeddings after 42 convolution layers  $\mathcal{F}_{1:42}^{-1}(\mathcal{F}_{1:42}(\mathbf{x}))$ .



Recovered images from ResNet-50 (MoCo V2 [96]) feature embeddings after 42 convolution layers  $\mathcal{F}_{1:42}^{-1}(\mathcal{F}_{1:42}(\mathbf{x}))$ .

Figure 11: ImageNet inversion results without original data given only a pretrained ResNet-50 with changing training recipes (standard [24] and self-supervised [96]). Best viewed in color.

V2 [96]<sup>7</sup>. For this experiment, we break the overall ResNet-50 architecture into five sub-networks and invert one sub-network each time.

Same as ResNet-18, the first sub-network is the initial block. The other four sub-networks consist of 3, 4, 6, 3 Bottleneck's respectively [24].

Fig. 11 shows the main inversion results of ResNet-50 on ImageNet. We observe that a stronger feature extractor preserves more information - see a quick comparison between second and third rows in Fig. 11. Self-supervised pretraining leads to stronger inversion, when compared to a standard training recipe of the same network architecture. This is consistent with the recent findings in [99]. These results demonstrate that we are able to recover recognizable input images for up to 4 sub-networks, which have 42 convolution layers and one max pooling layer in total.

<sup>7</sup>Based on <https://github.com/facebookresearch/moco>.

## Limitations

We observe that the last convolution, pooling, and fully-connected layers remain lossy for inversion, which may stem from the fact that the network is pretrained heavily for the classification task. Yet, we observe inversion viability up to the 21-st convolutional block. This unveils that DNNs extract such a fertile amount of image-specific representation, that even pixel-wise recovery is viable.

## Conclusions

We have shown feasibility of network inversion of deep models on complex datasets, while alleviating most constraints by prior work such as model, training, or dataset priors. Our zero-shot method unifies inversion of discriminate and generative inversion under one approach. We further presented extensive analysis of inversion behavior of large-scale networks, characterized their behaviours in filtering information, defending adversarial attacks, improving defective generation, and varying response to generated and real samples.

## Broader Impact

This work contributes to deeper understanding of DNNs' invertibility. We conducted a range of experiments to study the properties the inversion induces. This will help both research and industrial communities to investigate data security vulnerabilities of machine-learning-as-a-service and improve their pre-trained models. The method also reduces the amount of data required during inversion as compared to prior art, helping to alleviating environmental burdens at the same time.

## References

- [1] Andrew G Howard, Menglong Zhu, Bo Chen, Dmitry Kalenichenko, Weijun Wang, Tobias Weyand, Marco Andreetto, and Hartwig Adam. Mobilenets: Efficient convolutional neural networks for mobile vision applications. *arXiv preprint arXiv:1704.04861*, 2017. 1
- [2] Hong-Yen Chen and Chung-Yen Su. An enhanced hybrid mobilenet. In *2018 9th International Conference on Awareness Science and Technology (iCAST)*, pages 308–312. IEEE, 2018.
- [3] Li Deng, Geoffrey Hinton, and Brian Kingsbury. New types of deep neural network learning for speech recognition and related applications: An overview. In *2013 IEEE international conference on acoustics, speech and signal processing*, pages 8599–8603. IEEE, 2013.
- [4] Geoffrey Hinton, Li Deng, Dong Yu, George E Dahl, Abdel-rahman Mohamed, Navdeep Jaitly, Andrew Senior, Vincent Vanhoucke, Patrick Nguyen, Tara N Sainath, et al. Deep neural networks for acoustic modeling in speech recognition: The shared views of four research groups. *IEEE Signal processing magazine*, 29(6):82–97, 2012. 1
- [5] Xiangyu Zhang, Xinyu Zhou, Mengxiao Lin, and Jian Sun. Shufflenet: An extremely efficient convolutional neural network for mobile devices. In *Proceedings of the IEEE conference on computer vision and pattern recognition*, pages 6848–6856, 2018. 1
- [6] Song Han, Jeff Pool, John Tran, and William J Dally. Learning both weights and connections for efficient neural networks. *arXiv preprint arXiv:1506.02626*, 2015. 1
- [7] Yiping Kang, Johann Hauswald, Cao Gao, Austin Rovinski, Trevor Mudge, Jason Mars, and Lingjia Tang. Neurosurgeon. In *Proceedings of the Twenty-Second International Conference on Architectural Support for Programming Languages and Operating Systems*. ACM, 2017. 1, 7
- [8] Hyomin Choi and Ivan V Bajić. Deep feature compression for collaborative object detection. In *2018 25th IEEE International Conference on Image Processing (ICIP)*, pages 3743–3747. IEEE, 2018.
- [9] Robert A Cohen, Hyomin Choi, and Ivan V Bajić. Lightweight compression of neural network feature tensors for collaborative intelligence. In *2020 IEEE International Conference on Multimedia and Expo (ICME)*, pages 1–6. IEEE, 2020. 1
- [10] Hyuk-Jin Jeong, Inchang Jeong, Hyeon-Jae Lee, and Soo-Mook Moon. Computation offloading for machine learning web apps in the edge server environment. In *2018 IEEE 38th International Conference on Distributed Computing Systems (ICDCS)*. IEEE, 2018. 1, 7

- [11] Amir Erfan Eshratifar, Mohammad Saeed Abrishami, and Massoud Pedram. Jointdnn: an efficient training and inference engine for intelligent mobile cloud computing services. *IEEE Transactions on Mobile Computing*, 2019.
- [12] Guangli Li, Lei Liu, Xueying Wang, Xiao Dong, Peng Zhao, and Xiaobing Feng. Auto-tuning neural network quantization framework for collaborative inference between the cloud and edge. In *International Conference on Artificial Neural Networks*, pages 402–411. Springer, 2018.
- [13] Mikolaj Jankowski, Deniz Gündüz, and Krystian Mikołajczyk. Joint device-edge inference over wireless links with pruning. In *2020 IEEE 21st International Workshop on Signal Processing Advances in Wireless Communications (SPAWC)*, pages 1–5. IEEE, 2020.
- [14] Amir Erfan Eshratifar, Amirhossein Esmaili, and Massoud Pedram. Bottlenet: A deep learning architecture for intelligent mobile cloud computing services. In *2019 IEEE/ACM International Symposium on Low Power Electronics and Design (ISLPED)*, pages 1–6. IEEE, 2019. 1, 7
- [15] Amir Erfan Eshratifar, Mohammad Saeed Abrishami, and Massoud Pedram. Jointdnn: An efficient training and inference engine for intelligent mobile cloud computing services. *IEEE Transactions on Mobile Computing*, 20(2):565–576, 2021. 1
- [16] Daniele Jahier Pagliari, Roberta Chiaro, Enrico Macii, and Massimo Poncino. Crime: Input-dependent collaborative inference for recurrent neural networks. *IEEE Transactions on Computers*, 2020.
- [17] Yoshitomo Matsubara, Davide Callegaro, Sabur Baidya, Marco Levorato, and Sameer Singh. Head network distillation: Splitting distilled deep neural networks for resource-constrained edge computing systems. *IEEE Access*, 8:212177–212193, 2020.
- [18] Shuochao Yao, Jinyang Li, Dongxin Liu, Tianshi Wang, Shengzhong Liu, Huajie Shao, and Tarek Abdelzaher. Deep compressive offloading: speeding up neural network inference by trading edge computation for network latency. In *Proceedings of the 18th Conference on Embedded Networked Sensor Systems*, pages 476–488, 2020. 1
- [19] Sanjeev Arora, Yingyu Liang, and Tengyu Ma. Why are deep nets reversible: A simple theory, with implications for training. In *ICLR*, 2015. 1, 2, 3
- [20] Jörn-Henrik Jacobsen, Arnold Smeulders, and Edouard Oyallon. i-revnet: Deep invertible networks. *ICLR*, 2018. 1, 3
- [21] Qi Lei, Ajil Jalal, Inderjit S. Dhillon, and Alexandros G. Dimakis. Inverting deep generative models, one layer at a time. In *NeurIPS*, 2019. 1, 2, 3, 8
- [22] Robert Geirhos, Patricia Rubisch, Claudio Michaelis, Matthias Bethge, Felix A Wichmann, and Wieland Brendel. Imagenet-trained cnns are biased towards texture; increasing shape bias improves accuracy and robustness. *arXiv preprint arXiv:1811.12231*, 2018. 1
- [23] Vinod Nair and Geoffrey E Hinton. Rectified linear units improve restricted boltzmann machines. In *ICML*, 2010. 1
- [24] Kaiming He, Xiangyu Zhang, Shaoqing Ren, and Jian Sun. Deep residual learning for image recognition. *arXiv preprint arXiv:1512.03385*, 2015. 2, 3, 6, 9, 10
- [25] Xiaohan Ding, Xiangyu Zhang, Ningning Ma, Jungong Han, Guiguang Ding, and Jian Sun. Repvgg: Making vgg-style convnets great again. *CVPR*, 2021. 2, 6
- [26] Ian Goodfellow, Honglak Lee, Quoc Le, Andrew Saxe, and Andrew Ng. Measuring invariances in deep networks. *Advances in neural information processing systems*, 22:646–654, 2009. 2
- [27] Christian Szegedy, Wojciech Zaremba, Ilya Sutskever, Joan Bruna, Dumitru Erhan, Ian Goodfellow, and Rob Fergus. Intriguing properties of neural networks. *arXiv preprint arXiv:1312.6199*, 2013.
- [28] Xavier Glorot, Antoine Bordes, and Yoshua Bengio. Domain adaptation for large-scale sentiment classification: A deep learning approach. In *ICML*, 2011. 2
- [29] Anna C. Gilbert, Yi Zhang, Kibok Lee, Yuting Zhang, and Honglak Lee. Towards understanding the invertibility of convolutional neural networks. In *IJCAI*, 2017. 2, 3, 4
- [30] Jens Behrmann, Sören Dittmer, Pascal Fensel, and Peter Maaß. Analysis of invariance and robustness via invertibility of relu-networks. *arXiv preprint arXiv:1806.09730*, 2018. 2



- [31] Aviad Aberdam, Dror Simon, and Michael Elad. When and how can deep generative models be inverted? *arXiv preprint arXiv:2006.15555*, 2020. 2
- [32] Wen-Pu Cai and W. Li. Weight normalization based quantization for deep neural network compression. *ArXiv*, abs/1907.00593, 2019. 2, 3
- [33] Yuhang Li, Xin Dong, and W. Wang. Additive powers-of-two quantization: An efficient non-uniform discretization for neural networks. In *ICLR*, 2020. 2, 3
- [34] Alexey Dosovitskiy and Thomas Brox. Inverting visual representations with convolutional networks. In *CVPR*, 2016. 2, 3, 4
- [35] Anh Nguyen, Jeff Clune, Yoshua Bengio, Alexey Dosovitskiy, and Jason Yosinski. Plug & play generative networks: Conditional iterative generation of images in latent space. In *CVPR*, 2017. 3, 5, 9
- [36] Alexey Dosovitskiy and Thomas Brox. Generating images with perceptual similarity metrics based on deep networks. 2016. 3, 4, 5, 9, 17
- [37] Paul Hand, Oscar Leong, and Vladislav Voroninski. Phase retrieval under a generative prior. *arXiv preprint arXiv:1807.04261*, 2018. 2
- [38] Andrew Brock, Jeff Donahue, and Karen Simonyan. Large scale GAN training for high fidelity natural image synthesis. In *International Conference on Learning Representations*, 2019. 2, 3
- [39] Cicero Nogueira dos Santos, Youssef Mroueh, Inkit Padhi, and Pierre Dognin. Learning implicit generative models by matching perceptual features. In *Proceedings of the IEEE/CVF International Conference on Computer Vision*, pages 4461–4470, 2019. 2
- [40] Hongxu Yin, Pavlo Molchanov, Jose M. Alvarez, Zhizhong Li, Arun Mallya, Derek Hoiem, Niraj K Jha, and Jan Kautz. Dreaming to distill: Data-free knowledge transfer via deepinversion. In *CVPR*, 2020. 3, 5, 9, 17
- [41] Shoukai Xu, Haokun Li, Bohan Zhuang, Jing Liu, Jiezhong Cao, Chuangrun Liang, and Minghui Tan. Generative low-bitwidth data free quantization. In *European Conference on Computer Vision*, pages 1–17. Springer, 2020. 2, 5
- [42] Jia Deng, Wei Dong, Richard Socher, Li-Jia Li, Kai Li, and Li Fei-Fei. Imagenet: A large-scale hierarchical image database. In *2009 IEEE conference on computer vision and pattern recognition*, pages 248–255. Ieee, 2009. 2
- [43] Ziwei Liu, Ping Luo, Xiaogang Wang, and Xiaoou Tang. Deep learning face attributes in the wild. In *Proceedings of International Conference on Computer Vision (ICCV)*, December 2015. 2
- [44] Jens Behrmann, Will Grathwohl, Ricky TQ Chen, David Duvenaud, and Jörn-Henrik Jacobsen. Invertible residual networks. In *International Conference on Machine Learning*, pages 573–582. PMLR, 2019. 3
- [45] Will Grathwohl, Ricky TQ Chen, Jesse Bettencourt, Ilya Sutskever, and David Duvenaud. Ffjord: Free-form continuous dynamics for scalable reversible generative models. *ICLR*, 2018.
- [46] Jens Behrmann, Paul Vicol, Kuan-Chieh Wang, Roger Grosse, and Jörn-Henrik Jacobsen. Understanding and mitigating exploding inverses in invertible neural networks. In *International Conference on Artificial Intelligence and Statistics*, pages 1792–1800. PMLR, 2021.
- [47] Bo Chang, Lili Meng, Eldad Haber, Lars Ruthotto, David Begert, and Elliot Holtham. Reversible architectures for arbitrarily deep residual neural networks. In *Proceedings of the AAAI Conference on Artificial Intelligence*, volume 32, 2018. 3
- [48] Laurent Dinh, David Krueger, and Yoshua Bengio. Nice: Non-linear independent components estimation. *arXiv preprint arXiv:1410.8516*, 2014. 3
- [49] Laurent Dinh, Jascha Sohl-Dickstein, and Samy Bengio. Density estimation using real nvp. *arXiv preprint arXiv:1605.08803*, 2016.
- [50] Diederik P Kingma and Prafulla Dhariwal. Glow: Generative flow with invertible 1x1 convolutions. *arXiv preprint arXiv:1807.03039*, 2018. 3
- [51] Sanjeev Arora, Aditya Bhaskara, Rong Ge, and Tengyu Ma. Provable bounds for learning some deep representations. In *International conference on machine learning*, pages 584–592. PMLR, 2014. 3

- [52] Wenling Shang, Kihyuk Sohn, Diogo Almeida, and Honglak Lee. Understanding and improving convolutional neural networks via concatenated rectified linear units. In *international conference on machine learning*, pages 2217–2225. PMLR, 2016. 3
- [53] Fangchang Ma, Ulas Ayaz, and Sertac Karaman. Invertibility of convolutional generative networks from partial measurements. In *NeurIPS*, 2018. 3, 4
- [54] Piotr Teterwak, Chiyuan Zhang, Dilip Krishnan, and Michael C Mozer. Understanding invariance via feedforward inversion of discriminatively trained classifiers. *arXiv preprint arXiv:2103.07470*, 2021. 3, 5, 9
- [55] Alexander Mordvintsev, Christopher Olah, and Mike Tyka. Inceptionism: Going deeper into neural networks. <https://research.googleblog.com/2015/06/inceptionism-going-deeper-into-neural.html>, 2015. 3, 9, 17
- [56] Yaohui Cai, Zhewei Yao, Zhen Dong, Amir Gholami, Michael W Mahoney, and Kurt Keutzer. ZeroQ: A novel zero shot quantization framework. In *Proc. CVPR*, 2020.
- [57] Matan Haroush, Itay Hubara, Elad Hoffer, and Daniel Soudry. The knowledge within: Methods for data-free model compression. In *Proc. CVPR*, 2020.
- [58] Akshay Chawla, Hongxu Yin, Pavlo Molchanov, and Jose Alvarez. Data-free knowledge distillation for object detection. In *Proceedings of the IEEE/CVF Winter Conference on Applications of Computer Vision*, pages 3289–3298, 2021. 3
- [59] Pascal Vincent, Hugo Larochelle, Isabelle Lajoie, Yoshua Bengio, Pierre-Antoine Manzagol, and Léon Bottou. Stacked denoising autoencoders: Learning useful representations in a deep network with a local denoising criterion. *Journal of machine learning research*, 11(12), 2010. 3
- [60] Geoffrey E Hinton, Alex Krizhevsky, and Sida D Wang. Transforming auto-encoders. In *International conference on artificial neural networks*, pages 44–51. Springer, 2011. 3
- [61] Geoffrey E Hinton, Simon Osindero, and Yee-Whye Teh. A fast learning algorithm for deep belief nets. *Neural computation*, 18(7):1527–1554, 2006. 3
- [62] Yoshua Bengio, Pascal Lamblin, Dan Popovici, Hugo Larochelle, et al. Greedy layer-wise training of deep networks. *Advances in neural information processing systems*, 19:153, 2007. 3
- [63] Monica Bianchini and Franco Scarselli. On the complexity of neural network classifiers: A comparison between shallow and deep architectures. *IEEE transactions on neural networks and learning systems*, 25(8):1553–1565, 2014. 4
- [64] Ronen Eldan and Ohad Shamir. The power of depth for feedforward neural networks. In *Conference on learning theory*, pages 907–940. PMLR, 2016.
- [65] Matus Telgarsky. Benefits of depth in neural networks. In *Conference on learning theory*, pages 1517–1539. PMLR, 2016.
- [66] Maithra Raghu, Ben Poole, Jon Kleinberg, Surya Ganguli, and Jascha Sohl-Dickstein. On the expressive power of deep neural networks. In *international conference on machine learning*, pages 2847–2854. PMLR, 2017. 4
- [67] Richard Zhang, Phillip Isola, Alexei A. Efros, Eli Shechtman, and Oliver Wang. The unreasonable effectiveness of deep features as a perceptual metric. In *CVPR*, 2018. 4, 7
- [68] Jun-Yan Zhu, Taesung Park, Phillip Isola, and Alexei A Efros. Unpaired image-to-image translation using cycle-consistent adversarial networks. In *Proceedings of the IEEE international conference on computer vision*, pages 2223–2232, 2017. 4
- [69] Chun-Liang Li, Wei-Cheng Chang, Yu Cheng, Yiming Yang, and Barnabás Póczos. Mmd gan: Towards deeper understanding of moment matching network. *NeurIPS*, 2017. 5
- [70] Mikołaj Bińkowski, Dougal J Sutherland, Michael Arbel, and Arthur Gretton. Demystifying mmd gans. *ICLR*, 2018. 5
- [71] Alfred Müller. Integral probability metrics and their generating classes of functions. *Advances in Applied Probability*, pages 429–443, 1997. 5
- [72] Naveen Kodali, Jacob Abernethy, James Hays, and Zsolt Kira. On convergence and stability of gans. *arXiv preprint arXiv:1705.07215*, 2017. 5

- [73] Ngoc-Trung Tran, Viet-Hung Tran, Ngoc-Bao Nguyen, Trung-Kien Nguyen, and Ngai-Man Cheung. On data augmentation for gan training. *IEEE Transactions on Image Processing*, 30:1882–1897, 2021.
- [74] Shengyu Zhao, Zhijian Liu, Ji Lin, Jun-Yan Zhu, and Song Han. Differentiable augmentation for data-efficient gan training. In *Conference on Neural Information Processing Systems (NeurIPS)*, 2020. 5
- [75] Karen Simonyan and Andrew Zisserman. Very deep convolutional networks for large-scale image recognition. *arXiv preprint arXiv:1409.1556*, 2014. 6
- [76] Diederik P Kingma and Jimmy Ba. Adam: A method for stochastic optimization. *ICLR*, 2014. 6, 17
- [77] Peak signal-to-noise ratio. [https://en.wikipedia.org/wiki/Peak\\_signal-to-noise\\_ratio](https://en.wikipedia.org/wiki/Peak_signal-to-noise_ratio), 2021. 7
- [78] Jason Yosinski, Jeff Clune, Yoshua Bengio, and Hod Lipson. How transferable are features in deep neural networks? In Z. Ghahramani, M. Welling, C. Cortes, N. Lawrence, and K. Q. Weinberger, editors, *Advances in Neural Information Processing Systems*, volume 27. Curran Associates, Inc., 2014. 7, 17
- [79] Xingjian Li, Haoyi Xiong, Haozhe An, Cheng-Zhong Xu, and Dejing Dou. Rifle: Backpropagation in depth for deep transfer learning through re-initializing the fully-connected layer. In *International Conference on Machine Learning*, pages 6010–6019. PMLR, 2020.
- [80] Mingsheng Long, Yue Cao, Jianmin Wang, and Michael Jordan. Learning transferable features with deep adaptation networks. In *International conference on machine learning*, pages 97–105. PMLR, 2015.
- [81] Kaiming He Ross Girshick Piotr Dollár. Rethinking imagenet pre-training. 2018.
- [82] Barret Zoph, Golnaz Ghiasi, Tsung-Yi Lin, Yin Cui, Hanxiao Liu, Ekin D Cubuk, and Quoc V Le. Rethinking pre-training and self-training. *NeurIPS*, 2020. 7, 17
- [83] Kaiming He, Haoqi Fan, Yuxin Wu, Saining Xie, and Ross Girshick. Momentum contrast for unsupervised visual representation learning. In *Proceedings of the IEEE/CVF Conference on Computer Vision and Pattern Recognition*, pages 9729–9738, 2020. 7, 17
- [84] Jean-Bastien Grill, Florian Strub, Florent Althé, Corentin Tallec, Pierre H Richemond, Elena Buchatskaya, Carl Doersch, Bernardo Avila Pires, Zhaohan Daniel Guo, Mohammad Gheshlaghi Azar, et al. Bootstrap your own latent: A new approach to self-supervised learning. *arXiv preprint arXiv:2006.07733*, 2020.
- [85] Ting Chen, Simon Kornblith, Kevin Swersky, Mohammad Norouzi, and Geoffrey Hinton. Big self-supervised models are strong semi-supervised learners. *NeurIPS*, 2020. 7, 17
- [86] Aleksander Madry, Aleksandar Makelov, Ludwig Schmidt, Dimitris Tsipras, and Adrian Vladu. Towards deep learning models resistant to adversarial attacks. *ICLR*, 2017. 7
- [87] Alexey Kurakin, Ian Goodfellow, and Samy Bengio. Adversarial machine learning at scale. *ICLR*, 2016. 7
- [88] Ian Goodfellow, Jonathon Shlens, and Christian Szegedy. Explaining and harnessing adversarial examples. In *International Conference on Learning Representations*, 2015. 7
- [89] Nicholas Carlini and David Wagner. Adversarial examples are not easily detected: Bypassing ten detection methods. In *Proceedings of the 10th ACM Workshop on Artificial Intelligence and Security*, pages 3–14, 2017. 7
- [90] Kimin Lee, Kibok Lee, Honglak Lee, and Jinwoo Shin. A simple unified framework for detecting out-of-distribution samples and adversarial attacks. *NeurIPS*, 2018. 7
- [91] Takeru Miyato, Toshiki Kataoka, Masanori Koyama, and Yuichi Yoshida. Spectral normalization for generative adversarial networks. *ICLR*, 2018. 8
- [92] Tero Karras, Samuli Laine, Miika Aittala, Janne Hellsten, Jaakko Lehtinen, and Timo Aila. Analyzing and improving the image quality of stylegan. In *Proceedings of the IEEE/CVF Conference on Computer Vision and Pattern Recognition*, pages 8110–8119, 2020. 8
- [93] Wikipedia. Portable Network Graphics — Wikipedia, the free encyclopedia. <http://en.wikipedia.org/w/index.php?title=Portable%20Network%20Graphics&oldid=1022582831>, 2021. [Online; accessed 20-May-2021]. 8

- [94] Ruben Tolosana, Ruben Vera-Rodriguez, Julian Fierrez, Aythami Morales, and Javier Ortega-Garcia. Deepfakes and beyond: A survey of face manipulation and fake detection. *Information Fusion*, 64:131–148, 2020. 9
- [95] Robert Chesney and Danielle Keats Citron. Deep fakes: A looming challenge for privacy, democracy, and national security’ (2019). *California Law Review*, 107:1753, 2018. 9
- [96] Xinlei Chen, Haoqi Fan, Ross Girshick, and Kaiming He. Improved baselines with momentum contrastive learning. *arXiv preprint arXiv:2003.04297*, 2020. 9, 10
- [97] torchvision model zoos. <https://github.com/pytorch/vision/blob/master/torchvision/models>. 9
- [98] Joan Bruna Estrach, Arthur Szlam, and Yann LeCun. Signal recovery from pooling representations. In *International Conference on Machine Learning*, pages 307–315. PMLR, 2014. 9
- [99] See through gradients: Image batch recovery via gradinversion. In *Proceedings of the IEEE/CVF Conference on Computer Vision and Pattern Recognition*, 2021. 10
- [100] Cosineannealingwarmrestarts. [https://pytorch.org/docs/stable/optim.html?highlight=cosineannealingwarmrestarts#torch.optim.lr\\_scheduler.CosineAnnealingWarmRestarts](https://pytorch.org/docs/stable/optim.html?highlight=cosineannealingwarmrestarts#torch.optim.lr_scheduler.CosineAnnealingWarmRestarts). 17
- [101] Ilya Loshchilov and Frank Hutter. Sgdr: Stochastic gradient descent with warm restarts. *ICLR*, 2017. 17

## A Appendix

### A.1 Additional Details for Main Manuscript

**Lossy Final Fully-Connected Layer.** In the main manuscript, we show that the recovered images from RepVGG feature embeddings after 21 convolution layers preserve original semantic and visual attributes. However as we discuss in **Limitations**, we find that information in the feature embeddings decays rapidly through the last two layers in RepVGG. This may indicate that class-invariant information is quickly filtered out towards the end of the model while the initial stages focus on feature extraction, which is aligned with prior observations in transfer learning [78–82] and self-supervised learning [83–85]. We visualize the above findings in Fig. 12. One can still recognize the class of inverted images after the penultimate (*i.e.*, the 22-th convolution) layer. However, if we invert features after the final (*i.e.*, the fully-connected) layer, only the predominant color is recognizable.

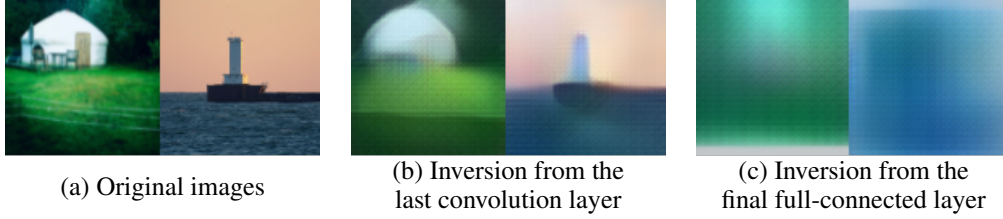


Figure 12: Results of inversion from the penultimate layer (*i.e.*, the last convolution layer (b)) and the final layer (*i.e.*, the final full-connected layer (c))

**Experiential Setup for Our Method.** For all experiments in the main manuscript, each inversion step is optimized via Adam [76] for 6K iterations. We set the initial learning rate as  $1 \cdot 10^{-3}$  during optimization of a certain inversion module  $\mathcal{F}_k^{-1}$  (3K iterations) and  $1 \cdot 10^{-4}$  during the following fine-tuning of all layer up to  $k$  such that  $\mathcal{F}_{1:k}^{-1} = \mathcal{F}_k^{-1} \circ \mathcal{F}_{1:(k-1)}^{-1}$  (3K iterations). We use cosine annealing with 3 warm restarts strategy to adjust the learning rate during optimization [100, 101]. The coefficient of cycle consistency loss  $\alpha$  in Equ. 4 is  $1 \cdot 10^{-7}$  to ensure it has similar magnitude as other loss terms. We use 5K synthetic images as detailed in Sec. 3.4 for the optimization.

**Experimental Setup for Prior Work.** We next elaborate on details for prior baselines:

- DeePSiM [36] learns a generator as inversion model which takes feature embeddings from target model as latent code and outputs recovered images. The generator is trained adversarially competing with an extra binary discriminator. For fair comparison, we replace the ImageNet training set used by [36] with 5K synthetic samples for optimization of inversion model.
- DeepDream [55] and DeepInversion [40] both back-propagate gradients onto inputs to optimize them towards natural images. For a fair comparison, we replace the CE loss in original setup [40, 55] and use  $\ell_2$  distance instead between synthesized and target embeddings to invert the same target layers as in the proposed method. We scale this loss to similar magnitudes as other loss terms with a scaling factor of  $1 \cdot 10^{-3}$ , other scaling terms the same as [40]. We study a randomly sampled validation batch of batch size 4 for this comparison. We use setting 2 that consumes 20K updates per batch as in [40] amid the requirement for feature map dimension consistency.